HHS Public Access

Author manuscript

Nat Neurosci. Author manuscript; available in PMC 2010 August 01.

Published in final edited form as:

Nat Neurosci. 2010 February ; 13(2): 205–212. doi:10.1038/nn.2464.

Control of hippocampal gamma oscillation frequency by tonic inhibition and excitation of interneurons

EO Mann and **I Mody**

Department of Neurology, David Geffen School of Medicine at the University of California, Los Angeles, California, 90095

Abstract

Gamma-frequency oscillations depend on phasic synaptic $GABA_A$ receptor-mediated inhibition to synchronize spike timing. The spillover of synaptically-released GABA can also activate extrasynaptic $GABA_A$ receptors, and such tonic inhibition may also contribute to modulating network dynamics. In many neuronal cell types, tonic inhibition is mediated by δ subunit-containing $GABA_A$ receptors. We show that the frequency of *in vitro* cholinergically-induced gamma oscillations in the mouse hippocampal CA3 region is increased by the activation of NMDA receptors (NMDAR) on interneurons. The NMDAR-dependent increase of gamma oscillation frequency is counteracted by the tonic inhibition of the interneurons mediated by δ subunit-containing $GABA_A$ receptors. Recordings of synaptic currents during gamma activity show that NMDAR-mediated increases in oscillation frequency correlate with a progressive synchronization of phasic excitation and inhibition in the network. Thus, the balance between tonic excitation and tonic inhibition of interneurons may modulate gamma frequency by shaping interneuronal synchronization.

Keywords

gamma oscillations; hippocampus; delta subunit; GABA; mouse

Gamma-frequency oscillations (γ oscillations; 30–120 Hz) have been recorded across a variety of cortical brain structures and behavioral states[1–3], and are thought to reflect coordinated spike timing in active neuronal networks. This rhythmic γ synchronization of neuronal activity has been suggested to play a role in several brain processes, including sensory encoding[4], neuronal assembly formation[5], and memory storage and retrieval[6,7]. Given that synaptic integration and plasticity are sensitive to the precise temporal correlations in spike times, the effects of γ oscillations on network function may depend on both the mechanism of synchronization and the specific oscillation frequency within the γ range. There is a broad consensus that the generation of γ oscillations depends on the rhythmic output of local networks of GABAergic interneurons, which synchronize the activity of excitatory neurons via phasic $GABA_A$ receptor-mediated inhibition[2,8–12].

Author Contributions: E.O.M. conducted the experiments and analysis. I.M. supervised the project. E.O.M. and I.M. wrote the manuscript.

Computational studies suggest further that the oscillation frequency can be tuned by altering the functional connectivity between excitatory and inhibitory neurons, the synaptic time constants and conduction delays10,13,14. However, the mechanisms by which the frequency of γ oscillations could be modulated dynamically within cortical circuits remain poorly understood.

Many insights into the mechanisms underlying γ rhythmogenesis have been gleaned from studying oscillations in the hippocampal CA3 recurrent network. In freely behaving rodents, γ oscillations in the CA3 are most commonly observed superimposed on theta-frequency oscillations (4–12 Hz), during exploratory behavior and rapid eye movement sleep1,15. These oscillations are also observed outside of theta episodes1, with a different class of 100–130 Hz oscillations emerging interspersed with sharp wave activity, and distinct from fast ripples16. Analogous fast oscillations can be induced in the CA3 network *in vitro* via activation of muscarinic acetylcholine receptors8 or kainate receptors17. These experimental models have suggested two mechanisms by which the phasic GABAergic inhibition onto pyramidal cells could itself be synchronized during γ oscillations. The entrainment of interneuronal firing within cholinergically-induced oscillations appears to depend on fast excitatory feedback from pyramidal cells8,9,18–20, while synchronization during kainate-induced oscillations may be generated autonomously within GABAergic networks21. A combination of phasic excitation, reciprocal GABAergic inhibition and electrical coupling are all likely to contribute to interneuronal synchronization during γ oscillations12,22–25. However, both *in vitro* models produce metronomic oscillations restricted to the low γ frequency range, leaving unanswered questions about the additional mechanisms required for the generation and modulation of higher frequency γ oscillations.

Synaptic $GABA_A$ receptor-mediated inhibition is critical for controlling spike timing during γ oscillations, but $GABA_A$ receptors are also located peri- and extra-synaptically. These receptors are activated by synaptic spillover26,27, and mediate tonic inhibitory currents that should affect network dynamics28,29. Tonic inhibition in CA3 pyramidal neurons is mediated predominantly byα5 subunit-containing $GABA_A$ receptors (α5-$GABA_A$R)30, and it has been shown that hippocampal slices from mice lacking α5-$GABA_A$R display larger amplitude γ oscillations, with no concomitant change in frequency31. In other neuronal cell types, such as granules cells in the dentate gyrus and cerebellum, tonic inhibition is mediated by δ subunit-containing $GABA_A$ receptors (δ-$GABA_A$R) receptors28,32. In the hippocampal CA3, δ-$GABA_A$R appear to be localized predominantly to GABAergic interneurons33, but their possible role in modulating cellular and network activity has yet to be explored. Here we show that hippocampal slices from adult δ subunit knockout mice display high-frequency carbachol-induced γ oscillations. This frequency-modulation results from a loss of tonic inhibition onto GABAergic interneurons, and a resulting increase in NMDAR-mediated excitation. A model of high-frequency γ oscillations in submerged juvenile slices, evoked by coactivation of cholinergic and NMDA receptors, was used to explore the cellular mechanisms in more detail.

Results

High-frequency hippocampal γ oscillations in *Gabrd−/−* mice

Cholinergic activation has previously been shown to induce ~40 Hz oscillations in the hippocampal CA3, which are dependent on synchronized inhibition8. To explore the possible role of δ-$GABA_A$R in modulating network activity in the hippocampal CA3, we analyzed the oscillations induced by 20 μM carbachol (CCh) in adult slices from *Gabrd*−/− and wildtype mice maintained in an interface chamber (Fig. 1). CCh-induced oscillations in *Gabrd*−/− mice had a peak frequency in the power spectrum of 64.8 ± 2.7 Hz (n = 8), which was significantly higher than that observed in wildtype slices of 43.9 ± 2.2 Hz (n = 8; $p < 0.001$). The frequency of CCh-induced oscillations could be reduced to wildtype levels by application of the NMDAR antagonist, 25 μM D-AP5 (37.4 ± 3.8 Hz; n = 6, $p < 0.001$ cf. control, p = 0.71 cf. WT), but blocking NMDAR had no significant effect on oscillation frequency in wildtype slices (44.3 ± 2.3 Hz; n = 5; two-way ANOVA followed by unpaired *t*-tests; Fig. 1a–**f**), as previously reported8. No significant differences in peak γ power were observed between genotypes (p = 0.082) or following NMDAR blockade (p = 0.104; two-way ANOVA; Fig. 1g).

The frequency of CCh-induced oscillations in *Gabrd*−/− mice varied over time (see Fig. 1a), and included bursts of high frequencies that were not obviously apparent in the power spectrum (see Fig. 1c). To analyze the frequency distribution of the CCh-induced oscillations in more detail, histograms of the instantaneous cycle frequency were created (Fig. 1e; see Methods). The incidence of high-frequency γ oscillations was quantified as the proportion of cycles with an instantaneous frequency above 60 Hz, which was found to be significantly higher for CCh-induced oscillations in slices from *Gabrd*−/− compared to WT mice (0.58 ± 0.04 vs 0.16 ± 0.01, $p < 0.001$), with this difference abolished following blockade of NMDAR ($p < 0.001$ cf. control, p = 0.77 cf. WT; two-way ANOVA followed by unpaired *t*-tests; Fig. 1h). This suggests that knocking out the δ subunit of $GABA_A$R unmasks an NMDAR-mediated current, which drives high-frequency γ oscillations following cholinergic activation.

To explore whether the CA3 network in adult wildtype slices could also support high-frequency γ oscillations, the ionic composition of the aCSF was modified to increase network excitability (1.2 mM $MgCl_2$, 3.5 mM KCl). Under these conditions, CCh-induced oscillations displayed a variety of peak frequencies ranging between those observed in wildtype and *Gabrd*−/− slices in normal aCSF (Supplementary Fig. 1). The frequency of γ oscillations in modified aCSF could be reduced by either blocking endogenous NMDAR activation or potentiating δ-$GABA_A$R with 100 nM THDOC (Supplementary Figs. 1 & 2), suggesting that a balance between NMDAR-and δ-$GABA_A$R-mediated currents could provide a common mechanism for controlling the frequency of γ oscillations.

Selectively reduced inhibition in *Gabrd−/−* CA3 interneurons

To determine the functional localization of δ-$GABA_A$R in the hippocampal CA3, spontaneous inhibitory postsynaptic currents (IPSCs) and tonic inhibitory currents were recorded from neurons in submerged slices, in the presence of 3 mM kynurenic acid to block

synaptic excitation (V_{hold} = −70 mV; CsCl-based internal solution). GABAergic currents were first recorded during baseline conditions, then the $GABA_AR$ agonist THIP (1 μM) was applied to the bath medium, and finally the tonic GABAergic current was calculated relative to the holding current following bath application of 20 μM gabazine or 50 μM picrotoxin at the end of the experiment (Fig. 2a,**b**).

Tonic GABAergic currents recorded from CA3 interneurons in the stratum oriens or radiatum, from slices of adult wildtype mice, were highly variable between cells, but could be detected in normal aCSF, and were consistently potentiated by 1 μM THIP (control: 18.8 ± 4.2 vs THIP: 29.9 ± 4.7 pA, n = 18; $p < 0.001$; Fig. 2a,c). The tonic currents in CA3 interneurons in *Gabrd*−/− mice were also increased by 1 μM THIP (3.6 ± 1.0 vs 10.0 ± 1.7 pA, n = 15; p = 0.002), but both the basal (p = 0.013) and THIP-induced currents (p = 0.0036) were significantly smaller than recorded in wildtypes (two-way repeated measures ANOVA followed by paired and unpaired *t*-tests, for the effects of THIP and genotype, respectively; Fig. 2b,c). The application of 1 μM THIP also affected sIPSCs, and, across both wildtype and *Gabrd*−/− mice, produced a small but significant increase in sIPSC frequency (14.7 ± 1.4 vs 17.8 ± 1.7 Hz, n = 33, $p < 0.001$) and decrease in sIPSC amplitude (37.9 ± 1.7 vs 35.9 ± 1.7 pA, n = 33, p = 0.006, two-way repeated measures ANOVA; Fig. 2c). However, these effects of THIP were unlikely to be mediated by δ-$GABA_AR$, as there were no significant interactions with genotype, and the only significant difference in sIPSCs between wildtype and *Gabrd*−/− mice was an overall reduction in sIPSC frequency (p = 0.024, two-way repeated measures ANOVA; Fig. 2c).

One possible reason for the variability in tonic currents recorded in wildtype CA3 interneurons could be an interneuronal subtype-specific expression of δ-$GABA_AR$. Three classes of interneuron were identified: i) perisomatic-targeting interneurons, with axon largely confined to the pyramidal cell layer, ii) dendritic-targeting interneurons, with axonal branching in the strata radiatum or lacunosum-moleculare, and iii) non-pyramidal projection neurons, whose axon was not confined to specific layers, and penetrated into the CA1 and/or dentate gyrus (Table 1; interneurons with incompletely recovered axons were excluded from this analysis). No significant differences were found in tonic currents between these cell types in wildtype slices (p = 0.54, one-way repeated measures ANOVA). Furthermore, there were no significant correlations between tonic currents recorded in interneurons and the properties of the sIPSCS, including mean amplitude, mean frequency and mean phasic current (r = −0.20 to −0.29, n = 18, p = 0.80 – 0.88, linear correlation; Fig. 2d). However, δ-$GABA_AR$ expression did appear to be cell-type specific. Recordings from pyramidal neurons showed a significant increase in tonic current and decrease in sIPSC amplitude in response to 1 μM THIP, but there were no significant differences between the GABAergic currents recorded in wildtype and *Gabrd*−/− mice (two-way repeated measures ANOVA followed by paired *t*-tests; Fig. 2d and Table 1), as previously reported30. This suggests that knocking out the δ-$GABA_AR$ results in a selective disinhibition of CA3 interneurons, largely due to a loss of tonic inhibition.

NMDAR-mediated excitation of *Gabrd−/−* CA3 interneurons

If NMDAR-dependent high-frequency CCh-induced oscillations in *Gabrd*−/− mice result from interneuronal disinhibition, then δ-$GABA_A$R-mediated tonic inhibition may normally act to curb the activation of NMDAR on interneurons. As the expression of δ-$GABA_A$R-mediated currents appeared variable across interneurons (see Fig. 2), and NMDAR-mediated currents are washed out readily in hippocampal interneurons during whole-cell recordings34, we tested for NMDA-evoked increases in sIPSCs onto CA3 pyramidal neurons in wildtype and *Gabrd*−/− mice (Fig. 3a). These experiments were performed in 20 μM DNQX to block AMPA/kainate receptor-mediated transmission. The bath application of 5 μM NMDA increased the mean phasic GABAergic current onto pyramidal neurons ($p = 0.001$), with a significantly larger increase in *Gabrd*−/− mice compared to wildtypes (WT: 10.8 ± 2.2 vs WT + NMDA: 17.5 ± 3.0 pA; *Gabrd*−/−: 15.2 ± 3.2 vs *Gabrd*−/− + NMDA: 37.1 ± 8.6 pA; $n = 10$ for each genotype, $p = 0.044$, two-way repeated measures ANOVA followed by unpaired *t*-test; Fig. 3b). This difference in mean phasic current was due predominantly to a greater increase in mean sIPSC amplitude ($p = 0.022$ cf. WT), rather than differences in the sIPSC frequency ($p = 0.67$; two-way repeated measures ANOVA; data not shown). To explore the subtype of NMDAR mediating these effects, experiments were repeated in the presence of 1 μM PPDA, a drug reported to preferentially antagonize NR2D-subunit containing NMDAR35. While the precise molecular composition of NMDAR on cortical GABAergic interneurons has yet to be elucidated, the possible role NR2D-subunit containing NMDAR was tested as hippocampal GABAergic interneurons show rich expression of this subunit relative to pyramidal neurons36,37. Indeed, 1 μM PPDA was found to completely inhibit the NMDA-evoked increases in the mean phasic GABAergic current in *Gabrd*−/− mice ($p = 0.53$, $n = 7$; paired *t*-test; Fig. 3c).

The application of 5 μM NMDA also induced a change in the holding current (I_{hold}) in pyramidal neurons ($p < 0.001$), which was not different between wildtype and *Gabrd*−/− mice ($p = 0.32$; two-way repeated measures ANOVA), but was not observed in the presence of 1 μM PPDA ($p = 0.78$; paired *t*-test; data not shown). The change in I_{hold} correlated significantly with change in sIPSC frequency ($r = 0.67$, $n = 27$, $p < 0.001$; linear correlation), but not the change in the mean phasic current or mean sIPSC amplitude ($r = 0.05$ and 0.01, $p = 0.59$ and 0.49, respectively; data not shown) and could reflect an NMDA-evoked increase in tonic inhibition. To confirm that the observed NMDAR-mediated effects were specific for interneurons, the experiments were first repeated in 20 μM gabazine to block $GABA_A$R. Unfortunately, under these conditions bath application of NMDA led to epileptiform bursts or runaway increases in I_{hold}, probably due to the strong recurrent excitatory connectivity between CA3 pyramidal cells. To overcome this problem, 5 μM ketamine was also included in the bath solution to block NMDAR, and this voltage-dependent block was relieved selectively in the recorded pyramidal neuron by holding it at +40 mV (drug cocktail: 20 μM DNQX, 20 μM gabazine, 5 μM ketamine; Cs-methylsulphonate based internal solution; Fig. 3d)38. The NMDA-evoked currents recorded in CA3 pyramidal neurons with this procedure, in *Gabrd*−/− mice, were not sensitive to 1 μM PPDA (control: 130 ± 22 vs PPDA: 144 ± 26 pA; $n = 7$ for each condition, $p = 0.68$; unpaired *t*-test; Fig. 3e). These data are consistent with CA3 GABAergic interneurons in

Gabrd−/− mice being selectively more sensitive to NMDAR-mediated excitation via PPDA-sensitive receptors.

To explore whether the activation of PPDA-sensitive NMDAR could account for the generation of high-frequency γ oscillations, we tested the NMDAR pharmacology of cholinergically-induced fast γ oscillations recorded in adult wildtype slices in modified aCSF. Indeed, 1 μM PPDA reduced the frequency of γ oscillations under these conditions of enhanced endogenous NMDAR activation (Supplementary Figs. 1 and 2).

Exogenous NMDAR activation increases γ frequency

To determine the mechanism by which NMDAR-mediated excitation of GABAergic interneurons could modulate the frequency of CCh-induced γ oscillations, the next aim was to induce oscillations under submerged conditions, which would allow simultaneous visualized patch-clamp recordings. Under these submerged conditions, we could only record CCh-induced oscillations in slices from juvenile mice (P14–21), with *Gabrd*−/− slices displaying only low-frequency γ oscillations, with a mean frequency of 40.5 ± 2.0 Hz, and with only a very low proportion of 0.04 ± 0.01 cycles having instantaneous frequencies above 60 Hz (n = 6; Fig. 4a–**f**). We found no differences between the network activity in juvenile *Gabrd*−/− and wildtpye slices, or effects of modifying the aCSF (data not shown).

The lack of genotypic affect on CCh-induced γ oscillations in juvenile slices most likely results from the late developmental expression of δ-$GABA_A$R in the hippocampus39. However, there are also clearly differences in neurotransmitter diffusion dynamics between submerged and interface conditions, so we tested whether exogenous activation of NMDAR could drive faster γ oscillations in these slices. Bath application of NMDA (1 – 7 μM) was found to produce a concentration-dependent increase in the peak frequency ($F_{4,42}$ = 17.0, p < 0.001) and the proportion of oscillatory cycles faster than 60 Hz ($F_{4,42}$ = 18.7, p < 0.001; Fig. 4a–**f**), with no significant differences between juvenile *Gabrd*−/− and wildtpye slices (frequency: $F_{1,42}$ = 1.12, p = 0.30; proportion cycles > 60 Hz: $F_{1,42}$ = 0.84, p = 0.37; two-way ANOVA; data from *Gabrd*−/− and WT slices combined for subsequent analysis). The application of 7 μM NMDA gave final values of 59.3 ± 2.1Hz (p < 0.001) and 0.33 ± 0.04 (p < 0.001, n = 7, post hoc unpaired *t*-test; Fig. 4f), respectively. This NMDA-evoked increase in frequency of CCh-induced oscillations was inhibited significantly by 0.1–1 μM PPDA (20 μM CCh + 5–7 μM NMDA before and after addition of 1 μM PPDA, frequency: 58.9 ± 2.6 vs 44.0 ± 2.9 Hz, proportion of cycles > 60 Hz: 0.32 ± 0.03 vs 0.11 ± 0.02, n = 5–6, p < 0.001, one-way ANOVA followed by unpaired *t*-test; Fig. 4g). Therefore, in submerged juvenile slices, exogenous application of NMDA was capable of invoking high-frequency γ oscillations via activation of PPDA-sensitive receptors, providing a novel *in vitro* model in which the mechanisms controlling γ frequency could be explored.

High-frequency γ depends on AMPAR-mediated excitation

Two principal mechanisms have been proposed to underlie γ oscillations – feedback loops between excitatory and inhibitory neurons, and oscillations within inhibitory interneuronal networks. CCh-induced fast oscillations in the hippocampal CA3 depend on AMPA receptor (AMPAR)-mediated excitation8,19, and have been suggested to be mediated by feedback

loops between pyramidal cells and GABAergic interneurons9. Bath application of the AMPAR-selective antagonist, 15–20 μM GYKI 53655, was also found to block the faster γ oscillations induced by co-application of 20 μM CCh and 5–7 μM NMDA (power in γ range: 960 ± 280 vs 140 ± 36 μV2, n = 5, p = 0.033, paired *t*-test; Fig. 5a–**c**). To determine whether an inhibitory oscillation might persist that was undetectable in the field potential, in three of these experiments simultaneous voltage-clamp recordings were made from CA3 pyramidal cells (Fig. 5d). With AMPAR-mediated excitation intact, both EPSCs and IPSCs showed rhythmicity, with peaks in the power spectrum and side peaks in the autocorrelation function (see Fig. 5e), corresponding to the frequency of the field potential oscillation (data not shown). Following application of 15–20 μM GYKI 53655, bursts of IPSCs could still be observed (Fig. 5d), but no rhythmicity could be observed for IPSCs within these bursts (Fig. 5e).

Reduced phase lag between EPSCs and IPSCs during high γ

It is possible that AMPAR-mediated excitation is not required for interneuronal synchronization *per se*, but rather to provide sufficient drive to enable oscillations in GABAergic networks, via direct excitation and/or the relief of the Mg^{2+} block of NMDAR. It is predicted that the synchronization of interneurons by phasic excitation would be associated with a synaptic delay between excitation and inhibition, whereas if interneurons were synchronizing both each other and pyramidal cells, then excitation and inhibition would be in phase in the network. Therefore, to distinguish between these mechanisms, the relationship between EPSCs and IPSCs was analyzed in CA3 pyramidal neurons from slices receiving varying amounts of exogenous excitatory drive (20 μM CCh + 1–7 μM NMDA; Fig 6a).

The peaks of both the EPSCs and IPSCs were significantly phase-coupled to the γ oscillation recorded in the field potential in all slices tested (r_{EPSC} = 0.31 – 0.72, r_{IPSC} = 0.23 – 0.80, n = 11 slices, p < 0.001, Rayleigh test for uniformity). The IPSCs were found to occur at a significantly later phase than the EPSCs (ϕ_{EPSC} vs ϕ_{IPSC} with [95 % confidence intervals]; modal phase: 1.42 [1.05, 1.78] vs 2.39 [2.17, 2.61] radians, $F_{1,20}$ = 24.9, p < 0.001, Watson-Williams test; mean phase: 1.72 [1.32, 2.21] vs 2.44 [2.00, 2.87] radians, $F_{1,9}$ = 22.5, p < 0.001, paired Hotelling test). This average difference in the timing of excitatory and inhibitory events was confirmed in the cross-correlations between the field potential and the PSCs (Fig. 6b), with the EPSCs displaying a lead of 4.8 ± 0.6 ms relative to the field oscillation, and the IPSCs displaying a lead of 0.6 ± 0.3 ms (n = 11, p < 0.001, paired *t*-test). However, the phase of the EPSCs and IPSCs varied significantly with the instantaneous oscillation frequency in each experiment (r = 0.14 – 0.37, n = 1022 - 4484 events; p < 0.001, angular-linear correlation), and there was a small but significant negative correlation between the difference in the EPSC-IPSC cross-correlation lags and the modal frequency of the field potential oscillation (r = −0.52, n = 11, p = 0.049, linear correlation).

To explore the frequency-dependence of synaptic-coupling in more detail, each oscillatory cycle was sorted into 15 Hz bins between 15 and 120 Hz according to instantaneous frequency. For visualization, frequency-binned average PSC waveforms were calculated, that were triggered on the negative peak of the field potential oscillation (Fig. 6c). For

quantification, if the PSCs within each frequency bin were significantly phase-locked to the field oscillation ($p < 0.05$, Rayleigh test for uniformity), then measurements were made of the phasic charge transfer per cycle (Fig. 6d), modal phase of the peak of the PSC (Fig. 6e), and the time lag between the negative peak in the field oscillation and the peak of the PSC (Fig. 6f). Phase-locked EPSCs were observed in only 5/11 cells in the 75–90 Hz range and 1/11 cells in the 90–105 Hz range. For the same frequency ranges, phase-locked IPSCs were observed in 8/11 and 3/11 cells, respectively. No significant phase-locking of PSCs was observed for instantaneous cycle frequencies between 105–120 Hz. For significantly phase-locked PSCs, there was a decrease in the charge transfer per cycle as the instantaneous frequency increased ($F_{1,92} = 11.3$ for effect of frequency, $p < 0.001$), and a loss of the dominance of inhibition over excitation ($F_{5,92} = 15.5$ for difference between PSCs, $p < 0.001$; $F_{5,92} = 2.47$ for interaction, $p = 0.042$; two-way ANOVA, see Fig. 6d for post-hoc analysis). This was associated with frequency dependent decrease in both the phase delays between the peaks of the EPSCs and IPSCs (Watson-Williams tests for each frequency bin, see Fig. 6e for p values), and the time lags between EPSCs and IPSCs ($F_{5,92} = 3.22$ for interaction between frequency and delay, $p = 0.010$, two-way ANOVA, see Fig. 6f for post-hoc analysis). Together, these findings suggest that as the frequency of γ oscillations increases, excitation and inhibition became more in phase and balanced.

Discussion

The initial finding of our study was that knocking out δ-$GABA_A$R leads to an increase in the frequency of cholinergically-induced γ oscillations in the adult hippocampal CA3 *in vitro*, which is dependent on the activation of NMDAR. We have provided further insights into the mechanisms underlying this change in CA3 network dynamics by showing that the modulation of the frequency results from the momentary balance between interneuronal tonic excitation by specific NR2D subunit-containing NMDAR and tonic inhibition mediated by δ-$GABA_A$R. We further show that: i) interneurons from *Gabrd*−/− mice display a reduction in tonic GABAergic inhibition, which enhances their sensitivity to NMDAR-mediated excitation, ii) slight enhancement of excitability (1.2 mM $MgCl_2$, 3.5 mM KCl) causes interneurons of WT slices to be sensitive to activation of NMDAR and thus contribute to enhanced oscillation frequency, iii) the frequency of cholinergically-induced oscillations in the juvenile hippocampal CA3 *in vitro* can be increased concentration-dependently by exogenous application of NMDA, and iv) during low-frequency γ oscillations there is a delay between phasic excitation and inhibition in the network, but this disappears with increasing oscillation frequency.

$GABA_A$R containing the δ subunit display high affinity, minimal desensitization, and are largely excluded from synaptic sites, and thus are most suited to transducing slow fluctuations in ambient GABA concentrations. Indeed, δ-$GABA_A$R have been shown to mediate such tonic inhibition in many cell types28,32, and are also expressed by interneurons in the hippocampus proper33. However, tonic inhibitory currents recorded previously in CA1 stratum radiatum interneurons have been reported to be sensitive to zolpidem27, which implies that the underlying $GABA_A$R contain the mutually-exclusive γ subunit. Here, we show that knocking out the δ subunit leads to a large reduction in tonic inhibition in CA3 interneurons, without changes in the tonic inhibition recorded in CA3

pyramidal neurons. Small residual tonic currents were observed in CA3 interneurons from *Gabrd*−/− mice, in response to both endogenous GABA release and THIP application, which could be mediated by γ subunit-containing $GABA_AR$. However, at least in hippocampal CA3, δ-$GABA_AR$ appear to play an important role in mediating reciprocal tonic inhibition within GABAergic networks.

A selective reduction in tonic inhibition across GABAergic interneurons might be expected to enhance synaptic GABA release through increases in the spontaneous spike rate27, and possible electrotonic changes in the membrane potential of presynaptic terminals40. Such changes are likely to be small when the excitatory drive is blocked pharmacologically, as the reversal potential for $GABA_AR$ appears to be close to the resting membrane potential in hippocampal interneurons10,41. We actually observed an overall reduction in the sIPSC frequency onto interneurons in *Gabrd*−/− relative to wildtype mice. This difference in sIPSCs was not observed in CA3 pyramidal neurons30, suggesting that it does not reflect a general decrease in spontaneous interneuronal activity in *Gabrd*−/− mice. One explanation would that the loss of the δ subunit leads to a selective reduction in spontaneous GABA release from interneuron-selective interneurons. We did not observe any differences in tonic GABAergic currents between interneuronal subtypes, but cannot rule out interneuronal-specific differences in δ-$GABA_AR$ expression or the $GABA_AR$ reversal potential. Alternatively, there could be a loss of putative presynaptic δ-$GABA_AR$ that normally act to enhance basal GABA releasese42, or adaptive changes in these mutant mice. While we cannot identify the precise mechanisms underlying the changes in IPSC frequency in *Gabrd* −/− mice, the dominant reduction in tonic inhibition of the CA3 interneurons is likely to be largely responsible for the associated changes in network dynamics, as reducing the reciprocal phasic inhibition between interneurons has little effect on the frequency of hippocampal γ oscillations24.

At the cellular level, tonic inhibition has been proposed to control neuronal excitability and output gain in response to excitatory inputs43. In this study, we show that tonic inhibition also plays a role in controlling the activation of voltage-dependent NMDAR. The increase in NMDA-evoked inhibition onto CA3 pyramidal neurons in *Gabrd*−/− mice was found to be blocked by PPDA, at concentrations reported to preferentially antagonize NR2D-subunit containing NMDAR35,44,45. This result is consistent with the expression of NR2D subunits in hippocampal GABAergic interneurons36,37. NR2D-subunit containing NMDAR have also been reported on CA1 pyramidal neurons44 and dentate granule cells45, but we found no evidence for tonic PPDA-sensitive NMDA currents in CA3 pyramidal neurons, confirming that the action of PPDA was directly on interneurons. Interestingly, NR2D-subunit containing NMDAR have been reported to have slow kinetics36,46 and be localized to the extrasynaptic membrane44–46. This suggests an attractive hypothesis, whereby slow extrasynaptic NMDAR-mediated excitation of interneurons could be balanced by tonic GABAergic inhibition.

The increased sensitivity of CA3 interneurons to NMDAR activation, following a reduction in the tonic inhibition, was associated with an increase in the frequency of cholinergically-induced γ oscillations recorded from adult slices in interface conditions. This effect could be mimicked in wildtype slices by modifying the aCSF, to enhance activation of NMDAR of

interneurons. Interestingly, non-desensitizing kainate receptors could not replace this function of NMDAR. Although kainate (100–200 nM) and carbachol induced similar fast γ oscillations in *Gabrd*−/− slices and in wildtype slices in modified aCSF, the increased frequencies were always dependent on NMDAR activation (Supplementary Figs. 3a-f). While NMDAR are not involved in the generation of low-frequency γ oscillations in hippocampal slices8, it has been shown that blocking NMDAR reduces the frequency of γ oscillations in slices of entorhinal cortex from ~40 Hz to ~30 Hz, due to a switch in the interneuronal subtypes recruited47. It seemed unlikely that the recruitment of a distinct cell type could explain our observed NMDAR-dependent increases in γ frequency, as most hippocampal interneuronal subtypes show γ phase-coupling *in vitro*18,20 and *in vivo*48, with synchronization of low-frequency γ oscillations already thought to depend on perisomatic-targeting interneurons with the fastest synaptic and intrinsic kinetics18–20,25. However, modeling studies have suggested that oscillation frequency can also change depending on the mechanism of interneuronal synchronization, with autonomous inhibitory networks able to oscillate at higher frequencies than those synchronized by fast feedback excitation form pyramidal neurons10,12–14,25.

To explore these mechanisms in more detail, we looked at faster γ oscillations induced by cholinergic and NMDAR activation in juvenile slices under submerged conditions, to enable simultaneous visualized patch-clamp recordings. In these slices, we found no significant differences in network activity between *Gabrd*−/− and wildtype mice, suggesting that δ-$GABA_A$R did not exert control over NMDAR activation in this preparation, probably due to the late developmental expression of δ-$GABA_A$R in the hippocampus39. However, the γ oscillations recorded in juvenile slices provided a model to explore the mechanisms by which NMDAR activation modulates network dynamics. We found that blocking AMPAR abolished all γ activity in the field potential, accompanied by a loss of rhythmic IPSCs recorded in pyramidal neurons, indicating that oscillations across the γ range depend on excitatory drive form pyramidal cells. To determine whether excitation was also important for synchronizing interneuronal firing, we examined the timing of synaptic events in pyramidal neurons, to test whether IPSCs occurred with a delay relative to EPSCs14. We found that synaptic inhibition lagged excitation during epochs of low-frequency γ oscillations, but that inhibition and excitation became progressively synchronized with increasing oscillation frequency. Similar results were obtained for the NMDAR modulation of kainate (200 nM) induced γ oscillations in juvenile slices under submerged conditions (Supplementary Figs. 3g-i), again suggesting a distinct role for NMDAR in shaping interneuronal synchronization. It is likely that NMDAR activation reduces spike latencies in the network, via changes in both membrane potential and integrative time constants, and could thus allow feedback loops between pyramidal cells and interneurons to generate a variety of frequencies within the same network. However, the timing of synaptic events at higher frequencies was not consistent with synaptic delays, which suggests that sufficient NMDAR activation might enable interneurons to escape phasic excitation, and synchronize within inhibitory networks.

The frequency of γ oscillations in the hippocampal CA3 can vary between 30–120 Hz in behaving animals1,5,15,16, but only oscillations in the low-frequency γ band have been

observed previously in reduced slice preparations. Here we show that the balance between tonic NMDAR-mediated excitation and δ-$GABA_A$R-mediated inhibition shapes interneuronal synchronization in mature circuits *in vitro*, and enables γ frequency-modulation. Further experiments will be required to determine whether similar mechanisms control γ frequency in the hippocampus *in vivo.* It is important to understand these mechanisms underlying the frequency-modulation of γ oscillations, as synaptic plasticity is known to be sensitive to the temporal correlations in spike times across the network. Indeed, changing the balance between tonic excitation and inhibition, via modulators of NMDAR/δ-$GABA_A$R, such as ethanol and neurosteroids32,49, and even NMDAR antagonists, might alter learning through effects on fast oscillatory dynamics.

Supplementary Material

Refer to Web version on PubMed Central for supplementary material.

Acknowledgments

This research was funded by the Epilepsy Foundation Postdoctoral Fellowship to E.O.M. and US National Institutes of Health grants NS30549, NS02808, and the Coelho Endowment to I.M.

References

1. Csicsvari J, Jamieson B, Wise KD, Buzsaki G. Mechanisms of gamma oscillations in the hippocampus of the behaving rat. Neuron. 2003; 37:311–322. [PubMed: 12546825]
2. Hasenstaub A, et al. Inhibitory postsynaptic potentials carry synchronized frequency information in active cortical networks. Neuron. 2005; 47:423–35. [PubMed: 16055065]
3. Steriade M, Amzica F, Contreras D. Synchronization of fast (30–40 Hz) spontaneous cortical rhythms during brain activation. J Neurosci. 1996; 16:392–417. [PubMed: 8613806]
4. Singer W. Synchronization of cortical activity and its putative role in information processing and learning. Annu Rev Physiol. 1993; 55:349–374. [PubMed: 8466179]
5. Montgomery SM, Buzsaki G. Gamma oscillations dynamically couple hippocampal CA3 and CA1 regions during memory task performance. Proc Natl Acad Sci U S A. 2007; 104:14495–500. [PubMed: 17726109]
6. Fell J, et al. Human memory formation is accompanied by rhinal-hippocampal coupling and decoupling. Nat Neurosci. 2001; 4:1259–1264. [PubMed: 11694886]
7. Lisman JE, Idiart MA. Storage of 7 +/− 2 short-term memories in oscillatory subcycles. Science. 1995; 267:1512–1515. [PubMed: 7878473]
8. Fisahn A, Pike FG, Buhl EH, Paulsen O. Cholinergic induction of network oscillations at 40 Hz in the hippocampus in vitro. Nature. 1998; 394:186–189. [PubMed: 9671302]
9. Traub RD, et al. A model of gamma-frequency network oscillations induced in the rat CA3 region by carbachol in vitro. Eur J Neurosci. 2000; 12:4093–4106. [PubMed: 11069606]
10. Vida I, Bartos M, Jonas P. Shunting inhibition improves robustness of gamma oscillations in hippocampal interneuron networks by homogenizing firing rates. Neuron. 2006; 49:107–17. [PubMed: 16387643]
11. Whittington MA, Traub RD, Jefferys JG. Synchronized oscillations in interneuron networks driven by metabotropic glutamate receptor activation. Nature. 1995; 373:612–615. [PubMed: 7854418]
12. Mann EO, Paulsen O. Role of GABAergic inhibition in hippocampal network oscillations. Trends Neurosci. 2007; 30:343–9. [PubMed: 17532059]
13. Wang XJ, Buzsaki G. Gamma oscillation by synaptic inhibition in a hippocampal interneuronal network model. J Neurosci. 1996; 16:6402–13. [PubMed: 8815919]

14. Brunel N, Wang XJ. What determines the frequency of fast network oscillations with irregular neural discharges? I. Synaptic dynamics and excitation-inhibition balance. J Neurophysiol. 2003; 90:415–30. [PubMed: 12611969]
15. Bragin A, et al. Gamma (40–100 Hz) oscillation in the hippocampus of the behaving rat. J Neurosci. 1995; 15:47–60. [PubMed: 7823151]
16. Csicsvari J, Hirase H, Czurko A, Mamiya A, Buzsaki G. Fast network oscillations in the hippocampal CA1 region of the behaving rat. J Neurosci. 1999; 19:RC20. [PubMed: 10436076]
17. Hajos N, et al. Cannabinoids inhibit hippocampal GABAergic transmission and network oscillations. Eur J Neurosci. 2000; 12:3239–49. [PubMed: 10998107]
18. Hajos N, et al. Spike timing of distinct types of GABAergic interneuron during hippocampal gamma oscillations in vitro. J Neurosci. 2004; 24:9127–37. [PubMed: 15483131]
19. Mann EO, Suckling JM, Hajos N, Greenfield SA, Paulsen O. Perisomatic feedback inhibition underlies cholinergically induced fast network oscillations in the rat hippocampus in vitro. Neuron. 2005; 45:105–17. [PubMed: 15629706]
20. Oren I, Mann EO, Paulsen O, Hajos N. Synaptic currents in anatomically identified CA3 neurons during hippocampal gamma oscillations in vitro. J Neurosci. 2006; 26:9923–34. [PubMed: 17005856]
21. Fisahn A, et al. Distinct roles for the kainate receptor subunits GluR5 and GluR6 in kainate-induced hippocampal gamma oscillations. J Neurosci. 2004; 24:9658–68. [PubMed: 15509753]
22. Fuchs EC, et al. Recruitment of parvalbumin-positive interneurons determines hippocampal function and associated behavior. Neuron. 2007; 53:591–604. [PubMed: 17296559]
23. Hormuzdi SG, et al. Impaired electrical signaling disrupts gamma frequency oscillations in connexin 36-deficient mice. Neuron. 2001; 31:487–495. [PubMed: 11516404]
24. Wulff P, et al. Hippocampal theta rhythm and its coupling with gamma oscillations require fast inhibition onto parvalbumin-positive interneurons. Proc Natl Acad Sci U S A. 2009; 106:3561–6. [PubMed: 19204281]
25. Bartos M, Vida I, Jonas P. Synaptic mechanisms of synchronized gamma oscillations in inhibitory interneuron networks. Nat Rev Neurosci. 2007; 8:45–56. [PubMed: 17180162]
26. Glykys J, Mody I. The main source of ambient GABA responsible for tonic inhibition in the mouse hippocampus. J Physiol. 2007; 582:1163–78. [PubMed: 17525114]
27. Semyanov A, Walker MC, Kullmann DM. GABA uptake regulates cortical excitability via cell type-specific tonic inhibition. Nat Neurosci. 2003; 6:484–90. [PubMed: 12679782]
28. Farrant M, Nusser Z. Variations on an inhibitory theme: phasic and tonic activation of GABA(A) receptors. Nat Rev Neurosci. 2005; 6:215–29. [PubMed: 15738957]
29. Semyanov A, Walker MC, Kullmann DM, Silver RA. Tonically active GABA A receptors: modulating gain and maintaining the tone. Trends Neurosci. 2004; 27:262–9. [PubMed: 15111008]
30. Glykys J, Mann EO, Mody I. Which GABA(A) receptor subunits are necessary for tonic inhibition in the hippocampus? J Neurosci. 2008; 28:1421–6. [PubMed: 18256262]
31. Towers SK, et al. Alpha 5 subunit-containing GABAA receptors affect the dynamic range of mouse hippocampal kainate-induced gamma frequency oscillations in vitro. J Physiol. 2004; 559:721–8. [PubMed: 15284346]
32. Glykys J, Mody I. Activation of GABAA receptors: views from outside the synaptic cleft. Neuron. 2007; 56:763–70. [PubMed: 18054854]
33. Peng Z, et al. GABA(A) receptor changes in delta subunit-deficient mice: altered expression of alpha4 and gamma2 subunits in the forebrain. J Comp Neurol. 2002; 446:179–97. [PubMed: 11932935]
34. Lamsa K, Irvine EE, Giese KP, Kullmann DM. NMDA receptor-dependent long-term potentiation in mouse hippocampal interneurons shows a unique dependence on Ca(2+)/calmodulin-dependent kinases. J Physiol. 2007; 584:885–94. [PubMed: 17884930]
35. Hrabetova S, et al. Distinct NMDA receptor subpopulations contribute to long-term potentiation and long-term depression induction. J Neurosci. 2000; 20:RC81. [PubMed: 10827202]

36. Monyer H, Burnashev N, Laurie DJ, Sakmann B, Seeburg PH. Developmental and regional expression in the rat brain and functional properties of four NMDA receptors. Neuron. 1994; 12:529–40. [PubMed: 7512349]
37. Standaert DG, Landwehrmeyer GB, Kerner JA, Penney JB Jr, Young AB. Expression of NMDAR2D glutamate receptor subunit mRNA in neurochemically identified interneurons in the rat neostriatum, neocortex and hippocampus. Brain Res Mol Brain Res. 1996; 42:89–102. [PubMed: 8915584]
38. MacDonald JF, et al. Actions of ketamine, phencyclidine and MK-801 on NMDA receptor currents in cultured mouse hippocampal neurones. J Physiol. 1991; 432:483–508. [PubMed: 1832184]
39. Laurie DJ, Wisden W, Seeburg PH. The distribution of thirteen GABAA receptor subunit mRNAs in the rat brain. III. Embryonic and postnatal development. J Neurosci. 1992; 12:4151–72. [PubMed: 1331359]
40. Alle H, Geiger JR. Combined analog and action potential coding in hippocampal mossy fibers. Science. 2006; 311:1290–3. [PubMed: 16513983]
41. Banke TG, McBain CJ. GABAergic input onto CA3 hippocampal interneurons remains shunting throughout development. J Neurosci. 2006; 26:11720–5. [PubMed: 17093093]
42. Trigo FF, Marty A, Stell BM. Axonal GABAA receptors. Eur J Neurosci. 2008; 28:841–8. [PubMed: 18691324]
43. Mitchell SJ, Silver RA. Shunting inhibition modulates neuronal gain during synaptic excitation. Neuron. 2003; 38:433–45. [PubMed: 12741990]
44. Lozovaya NA, et al. Extrasynaptic NR2B and NR2D subunits of NMDA receptors shape 'superslow' afterburst EPSC in rat hippocampus. J Physiol. 2004; 558:451–63. [PubMed: 15146049]
45. Harney SC, Jane DE, Anwyl R. Extrasynaptic NR2D-containing NMDARs are recruited to the synapse during LTP of NMDAR-EPSCs. J Neurosci. 2008; 28:11685–94. [PubMed: 18987204]
46. Misra C, Brickley SG, Farrant M, Cull-Candy SG. Identification of subunits contributing to synaptic and extrasynaptic NMDA receptors in Golgi cells of the rat cerebellum. J Physiol. 2000; 524(Pt 1):147–62. [PubMed: 10747189]
47. Middleton S, et al. NMDA receptor-dependent switching between different gamma rhythm-generating microcircuits in entorhinal cortex. Proc Natl Acad Sci U S A. 2008; 105:18572–7. [PubMed: 18997013]
48. Tukker JJ, Fuentealba P, Hartwich K, Somogyi P, Klausberger T. Cell type-specific tuning of hippocampal interneuron firing during gamma oscillations in vivo. J Neurosci. 2007; 27:8184–9. [PubMed: 17670965]
49. Nagy J. Alcohol Related Changes in Regulation of NMDA Receptor Functions. Curr Neuropharmacol. 2008; 6:39–54. [PubMed: 19305787]
50. Zar, JH. Biostatistical analysis. Prentice Hall; Upper Saddle River, N.J: 1999.

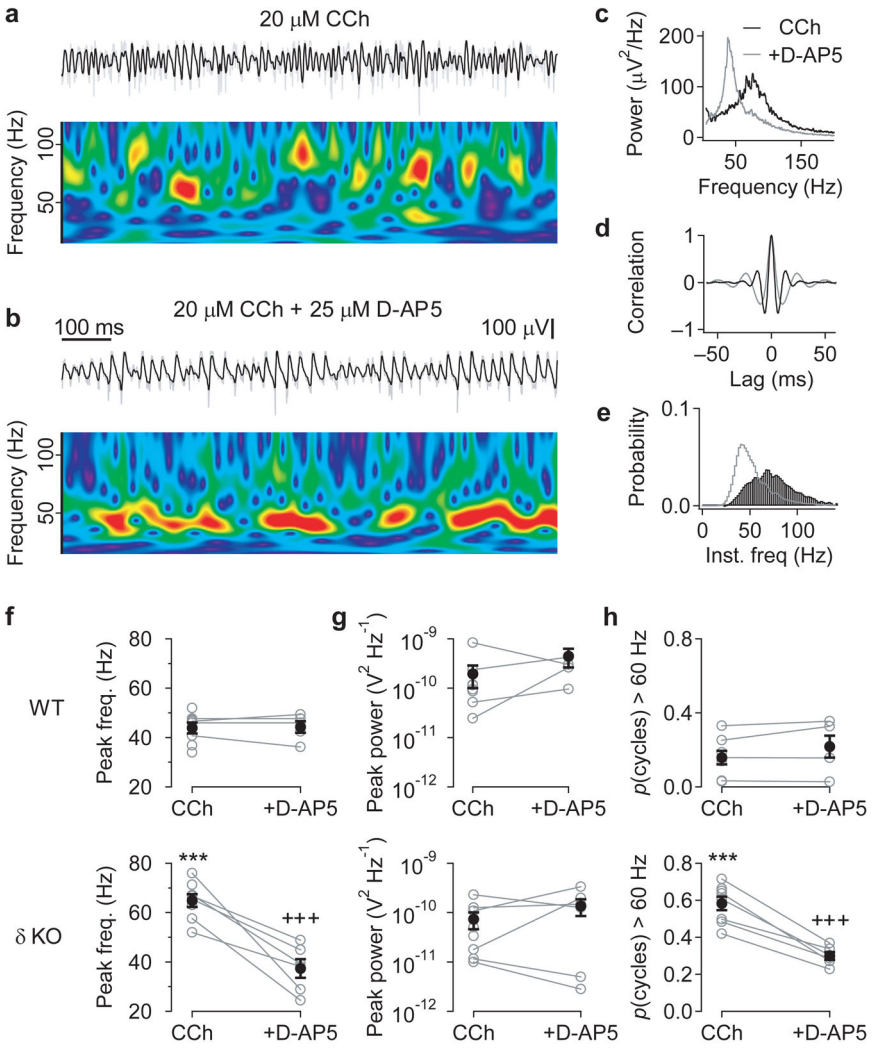

Figure 1. Cholinergic activation induces high-frequency γ oscillations in hippocampal slices from adult *Gabrd*−/− mice

(**a**) High-frequency γ oscillations induced by bath application of the cholinergic agonist, 20 μM carbachol, recorded extracellularly in the CA3 pyramidal cell layer from a hippocampal slice taken from an adult *Gabrd*−/− mouse. The upper traces show the field recording band-passed between 15 and 120 Hz (black), superimposed on the raw trace (grey). The wavelet spectrum below shows the variability in oscillation frequency over time (warmer colors indicate higher power). (**b**) Subsequent application of the NMDAR antagonist, 25 μM D-AP5, reduces oscillation frequency. Color scale for wavelet spectrum the same as in (a). (**c–e**) Properties of the oscillations induced by 20 μM carbachol (black) and following application of 25 μM D-AP5 (grey), from the experiment shown in a&b, compared using the power spectral density (c), autocorrelation (d) and histogram of the instantaneous cycle frequency (e). (**f–h**) Comparison of effects of D-AP5 on cholinergically-induced oscillations in slices from wildtype (WT, upper panels) and *Gabrd*−/− mice (lower panels), measured by the peak frequency in power spectral density (f), peak power (g), and proportion of cycles with an instantaneous frequency above 60 Hz (h). Slices from *Gabrd*−/− mice, but not

wildtype mice, displayed NMDAR-dependent high-frequency γ oscillations, without any significant differences in oscillation power (***p < 0.001 cf. WT, +++p < 0.001 cf. control, Two-way ANOVA followed by unpaired *t*-test, n = 5–8). Error bars represent s.e.m.

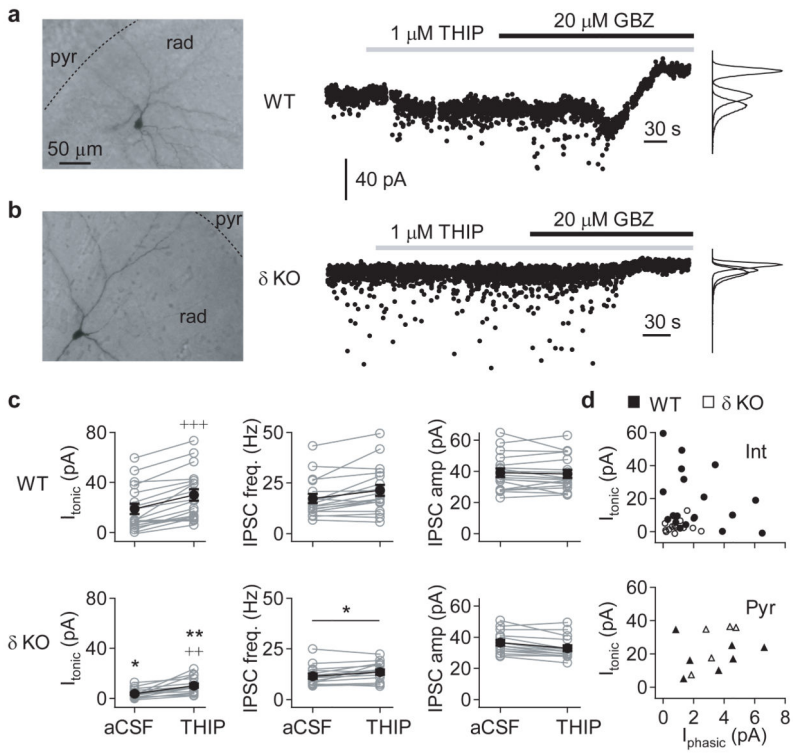

Figure 2. Hippocampal CA3 interneurons are disinhibited in adult *Gabrd*−/− mice

GABAergic currents in hippocampal CA3 neurons were recorded in whole-cell voltage-clamp mode (V_{hold} = −70 mV) in the presence of 3 mM kynurenic acid, using a CsCl-based pipette solution. The pipette solution also contained biocytin, which allowed post-hoc classification of cell type based on morphology. (**a**) Representative recording from a CA3 radiatum interneuron (left) from a wildtype mouse. GABAergic currents were recorded during baseline conditions, and following bath application of 1 μM THIP (middle), and the tonic GABAergic current calculated relative to the holding current following bath application of 20 μM gabazine, or 50 μM picrotoxin, at the end of the experiment. (**b**) Representative recording from a similar CA3 radiatum interneuron (left) from a *Gabrd*−/− mouse, as in panel (a). (**c**) Summary of GABAergic currents recorded in CA3 interneurons from adult wildtype (top) and *Gabrd*−/− mice (bottom), showing the tonic GABAergic current (I_{tonic}; left), frequency of spontaneous IPSCs (sIPSC; middle) and mean sIPSC amplitude (right), during both baseline conditions and following application of THIP. Error bars represent s.e.m. (**d**) Relationship between I_{tonic} and the mean phasic current (I_{phasic}) in 1 μM THIP for CA3 interneurons (upper) and pyramidal neurons (lower). (*p < 0.05, **p < 0.01 cf. WT, +++p < 0.001, ++p < 0.01 vs baseline, Two-way repeated measures ANOVA followed by unpaired and paired *t*-tests, respectively)

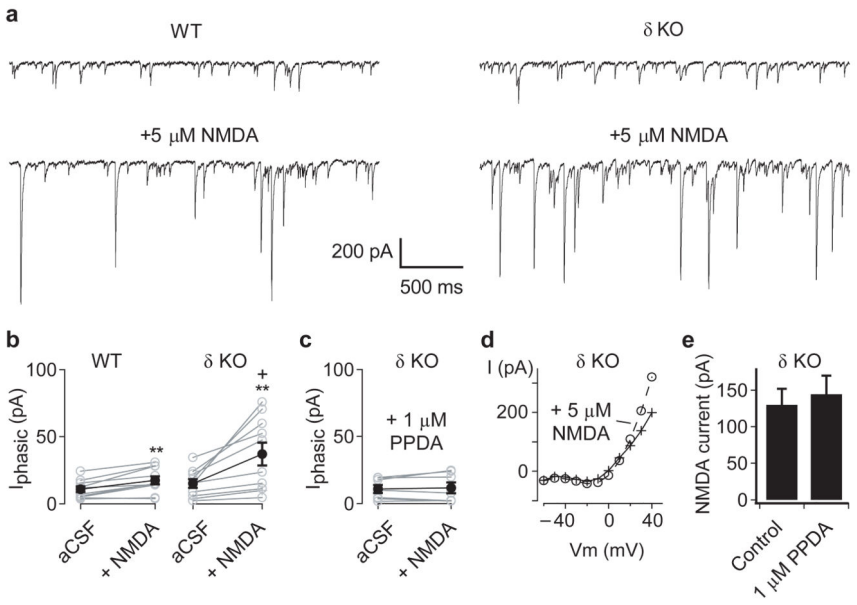

Figure 3. Hippocampal CA3 interneurons in adult *Gabrd*−/− mice are more sensitive to NMDAR-mediated excitation

(**a**) To monitor the output of inhibitory interneurons, GABAergic currents were recorded from CA3 neurons pyramidal neurons, in the presence of 20 μM DNQX, using a CsCl-based pipette solution. Representative traces show the spontaneous IPSCs recorded during baseline conditions (upper) and following bath application of 5 μM NMDA (lower), in slices from adult wildtype (left) and *Gabrd*−/− mice (right). (**b**) Application of 5 μM NMDA increased the mean phasic current (I_{phasic}) in both wildtype (left) and *Gabrd*−/− mice (right), with significantly larger increases in inhibition in the *Gabrd*−/− mice. (**c**) The NMDA-evoked increases in I_{phasic} in *Gabrd*−/− mice were blocked by 1 μM PPDA. (**d**) To determine whether PPDA might act indirectly by blocking NMDAR on pyramidal neurons, recordings of NMDA currents were obtained in the presence of 20 μM DNQX, 20 μM gabazine and 5 μM ketamine, using a Cs-methylsulphonate based internal solution. The current-voltage plot before and after application of 5 μM NMDA, in a single pyramidal neuron, shows the voltage-dependent relief of ketamine block of the NMDAR at +40 mV (e) Pooled data, showing that 1 μM PPDA had no effect on the NMDA-evoked current recorded at +40 mV. (*$p < 0.05$ cf. WT, ++$p < 0.01$ vs baseline, Two-way repeated measures ANOVA followed by unpaired and paired *t*-test, respectively). Error bars represent s.e.m.

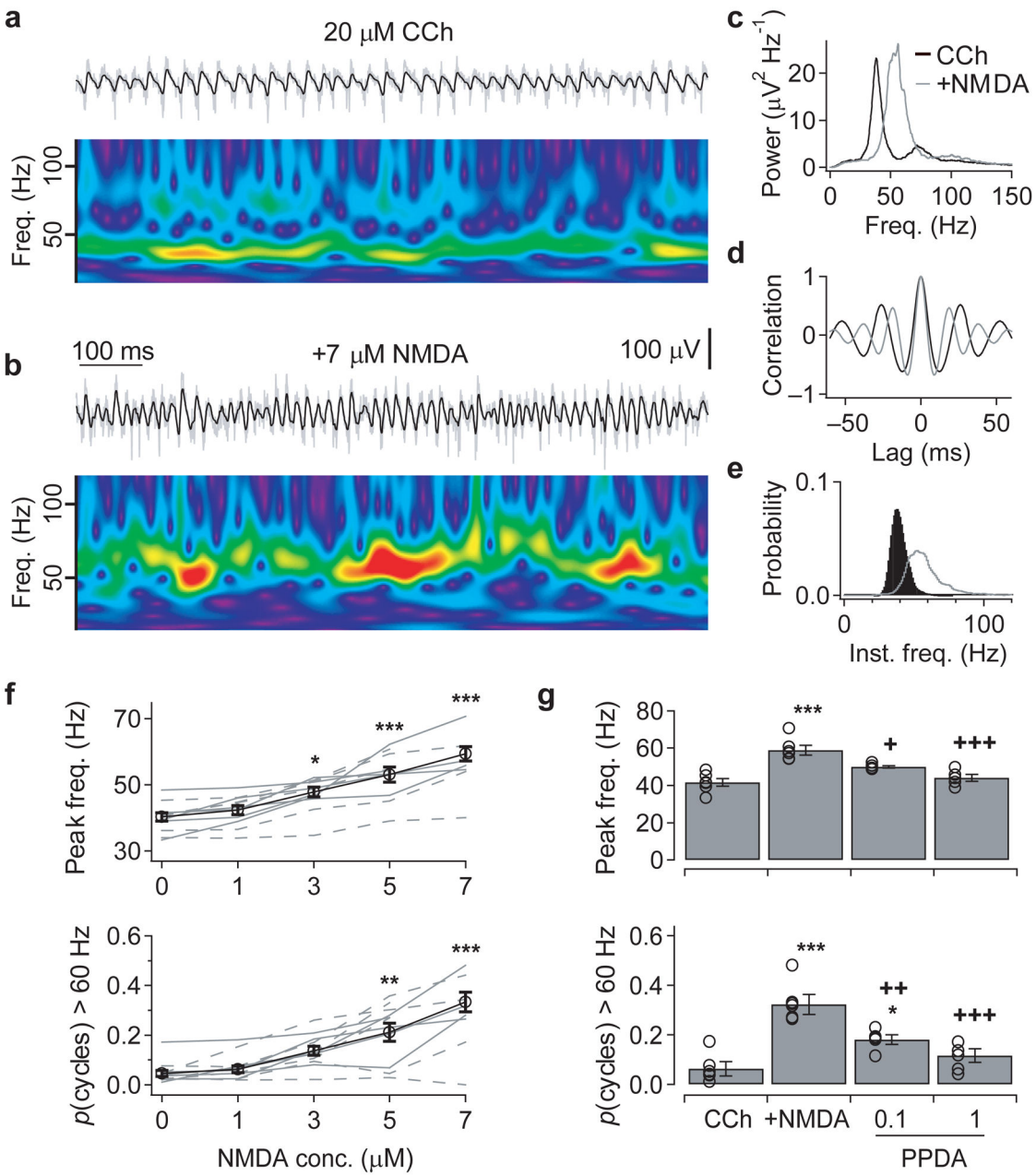

Figure 4. Activation of NMDAR increases the frequency of cholinergically-induced γ oscillations in juvenile slices

(**a&b**) To explore further the mechanisms underlying the frequency-modulation of γ oscillations, network activity was recorded in the submerged recording configuration, but it was only possible to induce oscillations in juvenile (P14–21) slices. Under these conditions, cholinergic activation (20 μM carbachol) induced oscillations in the low γ-frequency range in both *Gabrd*−/− and wildtype slices (a), but additional exogenous application of NMDA induced epochs of higher-frequency γ oscillations (b). The upper traces show the field recording from the CA3 pyramidal cell layer band-passed between 15 and 120 Hz (black), superimposed on the raw trace (grey). The wavelet spectrum below shows the oscillation

frequency over time (warmer colors indicate higher power, with same color scale used in both panels). (**c-e**) The NMDA-evoked increase in oscillation frequency, from the experiment shown in a&b, compared using the power spectral density (c), auto-correlation (d) and histogram of the instantaneous cycle frequency (e). (**f**) Exogenous NMDA application (1–7 μM) produced a concentration-dependent increase in peak oscillation frequency (upper) and the proportion of cycles with an instantaneous frequency above 60 Hz (lower) (solid lines: *Gabrd−/−*, dashed lines: wildtype; data combined for averages). (**g**) The 7 μM NMDA-evoked increases in oscillation frequency were blocked by the PPDA in a concentration-dependent manner. (*$p < 0.05$, **$p < 0.01$, ***$p < 0.001$ cf. control, +$p < 0.05$, ++$p < 0.01$, +++$p < 0.001$ cf. 5–7 μM NMDA, One-way ANOVA followed by unpaired *t*-test). Error bars represent s.e.m.

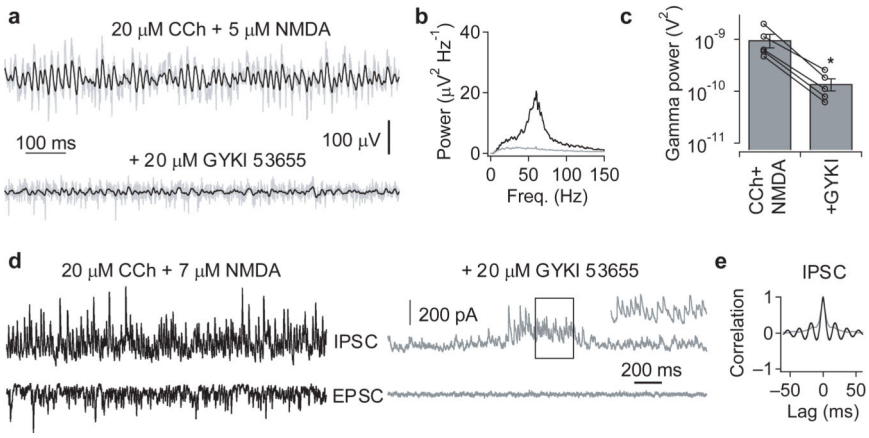

Figure 5. High-frequency γ oscillations depend on AMPAR-mediated excitation

(**a**) Oscillations induced in juvenile slices by the co-application of 20 μM carbachol and 5 μM NMDA (upper), were abolished by the AMPAR-selective antagonist, GYKI 53655 (20 μM; lower). The traces show the field recording from the CA3 pyramidal cell layer band-passed between 15 and 120 Hz (black), superimposed on the raw trace (grey). (**b&c**) Following blockade of AMPAR, no peaks were observable in the power spectral density (b), which was quantified as a significant reduction in the power in the in the 30–120 Hz range (c) (*$p < 0.05$, paired *t*-test for the effect of 15–20 μM GYKI 53655 on oscillations induced by 20 μM carbachol + 5–7 μM NMDA; n = 5). Error bars represent s.e.m. (**d**) Voltage-clamp recording of IPSCs (0 mV; upper) and EPSCs (−65 mV; lower) from a CA3 pyramidal neuron, showing that GYKI 53655 not only blocked phasic excitation, but also reduced phasic inhibition. Bursts of IPSCs could still be observed, and the inset shows a magnified run of IPSCs during a burst. (**e**) The autocorrelation for the IPSC recordings shown in (d), during both the ongoing oscillation (black) and bursts of IPSCs in the presence of GYKI (grey), showing that GYKI disrupts IPSC rhythmicity.

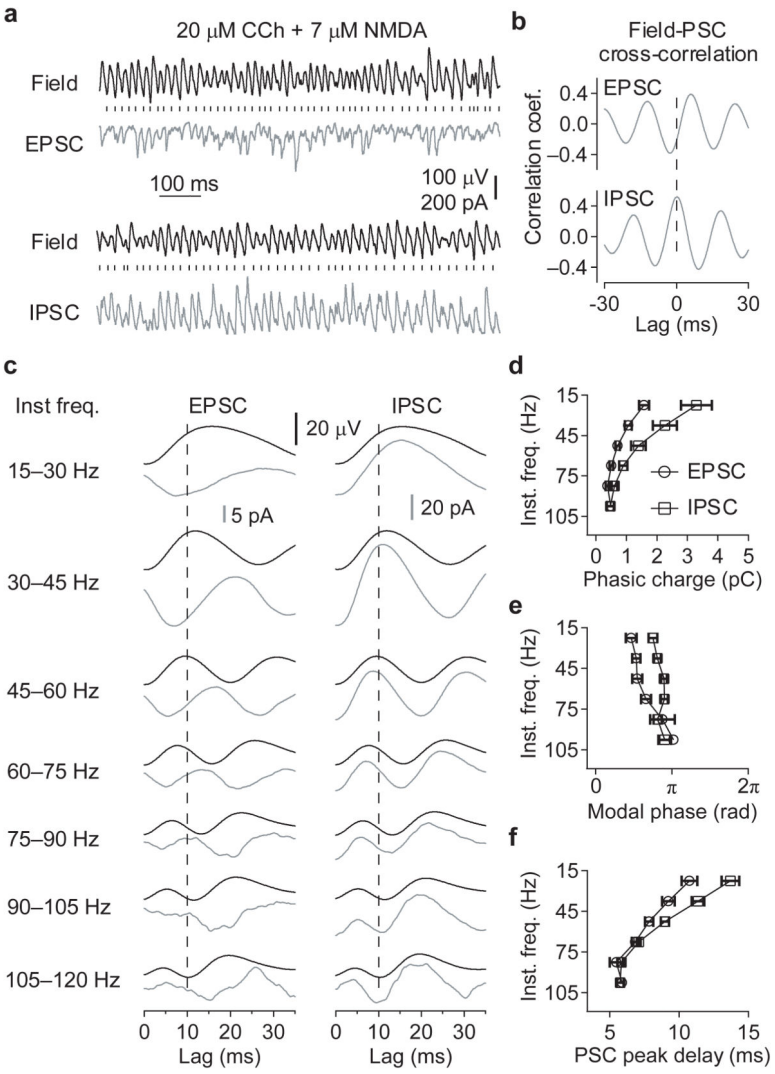

Figure 6. The lag between synaptic inhibition and excitation disappears as the γ oscillation frequency increases

(**a**) Representative traces showing the relationship between the field potential recorded from the CA3 pyramidal cell layer and the EPSCs and IPSCs recorded from a CA3 pyramidal neuron, during oscillations induced by co-application of 20 μM carbachol and 7 μM NMDA. The vertical dashes represent the zero phases (negative peaks) of the oscillation in the field potential. (**b**) Cross-correlations between synaptic currents and the field potential, showing that on average the EPSCs occur earlier in field potential oscillation cycle than the IPSCs. Dashed line represents zero lag. (**c**) Averages of the EPSC and IPSCwaveforms (grey), and corresponding field potential waveforms (black), triggered on the negative peak of the field potential oscillation, and separated into 15 Hz bins of according to instantaneous frequency. The polarity of the PSCs is the same as (a), with negative peaks in the EPSCs and positive peaks in the IPSCs. Data are combined from 11 recordings, with NMDA concentrations from 1–7 μM M to induce different γ oscillation frequencies. The vertical dashed lines mark a lag of 10 ms. (**d-f**) Charge transfer per oscillatory cycle (d), the modal phase of the peak

synaptic current (e), and lag of the peak synaptic current after the negative peak in field oscillations (f), binned as in (c). (n = 5–11, *p < 0.05, **p < 0.01, ***p < 0.001 EPSC vs IPSC, Two-way ANOVA followed by unpaired *t*-test; +p < 0.05, ++p < 0.01, +++p < 0.001 EPSC vs IPSC, Watson-Williams test). Error bars represent s.e.m.

Table 1

Properties of phasic and tonic GABAergic currents recorded from different cell types in wildtype and *Gabrd−/−* mice

Genotype	Cell type	n	IPSC frequency (Hz)	IPSC amplitude (pA)	THIP-induced I_{tonic} (pA)
WT	Pyramidal	8	18.8 ± 3.3	34.8 ± 2.9	19.8 ± 3.7
	Perisomatic-targeting interneuron	3	32.5 ± 6.5	40.2 ± 7.6	13.9 ± 6.2
	Dendritic-targeting interneuron	4	12.9 ± 8.6	31.2 ± 3.4	23.0 ± 9.4
	Non-pyramidal projection neuron	2	14.3 ± 2.4	53.4 ± 4.7	27.4 ± 15.1
δ KO	Pyramidal	5	17.2 ± 1.8	42.7 ± 2.6	25.8 ± 5.9
	Perisomatic-targeting interneuron	3	18.2 ± 3.8	40.5 ± 3.6	8.3 ± 2.4
	Dendritic-targeting interneuron	4	10.0 ± 1.7	37.1 ± 3.7	12.7 ± 4.5
	Non-pyramidal projection neuron	3	8.6 ± 0.5	38.4 ± 6.7	2.8 ± 5.7